Astronomy
&
Astrophysics

SED, age distribution and evolutionary history of M 33

J. Li, J. Ma, X. Zhou, Z. Jiang, Y. Yang, and J. Chen

National Astronomical Observatories, Chinese Academy of Sciences, Beijing 100012, PR China

Abstract. We present CCD spectrophotometry of the nearby spiral galaxy M 33 using images obtained with National Astronomical Observatories of China (NAOC) 60/90 cm Schmidt telescope in a broad U-band and 13 intermediate-band filters from 4000 to 10 000 Å. The observations cover the whole area of M 33, with a total integration of 39.08 h from September 23, 1995 to August 28, 2000. The spectral energy distributions (SEDs) for each area of M 33 are obtained. With the aid of an evolutionary synthesis model, PEGASE (Fioc & Rocca-Volmerange 1997, 2000), we compute theoretical SEDs for three kinds of star formation rate (SFR) histories. From best fits on templates of PEGASE and observed SEDs by the χ^2-minimization procedure, we find that both the constant and exponentially decreasing (hereafter Exp, $\tau = 12$ Gyr) SFR give good agreement between models and observations. We then obtain age distributions (when the observed stellar population formation began) and evolutionary histories of M 33 for the two models. For the constant SFR, an age gradient is clearly found between stellar populations of the central regions and of the outer regions. The stellar populations in its central regions are older than 10 Gyr; stars in the outer regions are younger, about 7 Gyr and the youngest components in the spiral arms are less than 5 Gyr. The Exp SFR gives a similar age distribution, but with absolute ages that are smaller by ∼2 Gyr. We conclude that M 33 has been forming stars continuously for most of its lifetime, with the interior having built up its stellar populations several Gyr earlier than the outer parts.

Key words. galaxies: individual: M 33 – galaxies: evolution – galaxies: stellar content

1. Introduction

As a small Scd Local Group galaxy, which is about 15 times farther from us than the LMC (distance modulus is 24.64), M 33 is interesting and important because it presents a morphological type intermediate between the largest "early-type" spiral galaxies and the dwarf irregulars in the Local Group (Freedman et al. 1991; Chandar et al. 1999). Because of its nearby location (840 kpc) (Freedman et al. 1991) and relatively face-on inclination (56°), M 33 has been an ideal galaxy for the study of galactic structure, yet its basic stellar morphology remains unclear. Observations of extragalactic HII regions can provide useful constraints on the physical process leading to formation of massive hot stars which are responsible for the chemical evolution of the interstellar medium. M 33, which is rich in HII regions, is an obvious candidate for such an investigation because of the extensive optical information now available. These objects, especially the brightest ones, have been the subject of a large number of papers, which have used them to study the composition, the abundance gradient, SFR and the mode of star formation (Hodge et al. 1999).

Our collaboration, the Beijing-Arizona-Taiwan-Connecticut (BATC) Multicolor Sky Survey (Fan et al. 1996; Zheng et al. 1999), had already observed this spiral galaxy as part of its galaxy calibration program. The BATC
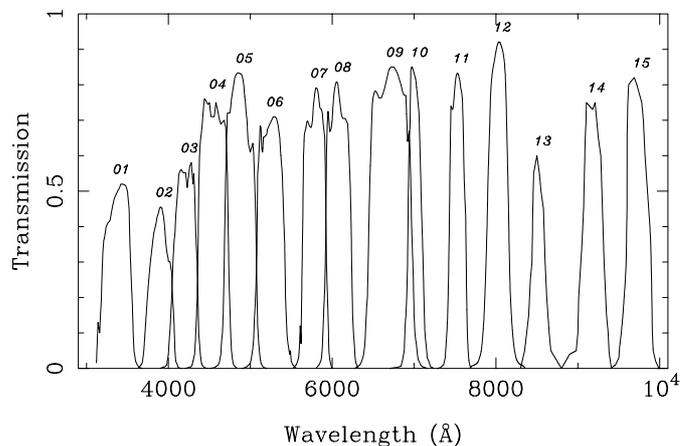
Fig. 1. The transmission curves of all the filters in BATC photometric system. The names of the filters are marked at the top of each curve. In this study, a U-band filter was used instead of the BATC01 and BATC02 filters.

program uses the 60/90 cm Schmidt telescope at the Xinglong Station of NAOC, with its focal plane equipped with a 2048 × 2048 Ford CCD and a set of 15 intermediate-band filters (Fig. 1) that was designed to obtain spectrophotometry for preselected 1 $\deg^2$ regions of the northern sky with this CCD system.

Since the pioneering work of Tinsley (1972) and Searle et al. (1973), evolutionary population synthesis has become a standard technique to study the stellar populations of galaxies. This is a result of improvements in the theory of the chemical evolution of galaxies, star formation, stellar evolution and atmospheres and of the development of synthesis algorithms and the availability of various evolutionary synthesis models. A comprehensive compilation of such models was presented by Leitherer et al. (1996) and Kennicutt (1998). More widely used models are those from the Padova and Geneva group (e.g. Schaerer & de Koter 1997; Schaerer & Vacca 1998; Bressan et al. 1996; Chiosi et al. 1998), GISSEL (Charlot & Bruzual 1991; Bruzual & Charlot 1993, 1996, 2003), PEGASE (Fioc & Rocca-Volmerange 1997) and STARBURST99 (Leitherer et al. 1999). Some theoretical tools, such as PEGASE, are now available, which can be used to interpret the spectra of galaxies. For example, PEGASE has been developed for instantaneous starburst, constant and exponentially decreasing (or increasing) star formation, and using this, one is able to derive the physical properties of a galaxy from the continuous spectrum. In this model, stellar initial mass function (IMF), star formation rate (SFR) and stellar atmosphere formulations are all adjustable initial parameters (Kewley et al. 2001).

As we know, multicolor photometry is able to provide accurate SEDs for galaxies. Since the Balmer Jump at 3650 Å can provide important information regarding the relative contribution of young FAB-type stars, U-band photometry is valuable as a means of characterizing stellar populations and star formation histories. In this paper, we present SEDs based on CCD imaging through a broad U-band and 13 intermediate-band filters. These SEDs are compared with results from stellar population evolutionary synthesis models to determine the spatial distribution of stellar ages in M 33 and the corresponding star formation histories.

Details of observations and data reduction are presented in Sect. 2. We provide a brief description of PEGASE in Sect. 3. In Sect. 4, age distributions and formation histories of M 33 for the constant and Exp SFR are obtained with a χ^2-minimization method. Comparison of BATC to the $UBVRI$ filter system is given in Sect. 5. Our main conclusions are summarized in Sect. 6.

2. Observations and data reduction

2.1. CCD image observation

Images of large-field multicolor observations of the spiral galaxy M 33 were obtained in the BATC photometric system. The BATC program uses the 60/90 cm f/3 Schmidt telescope at the Xinglong Station of NAOC, with a 2048×2048 Ford CCD mounted at its focal plane, and a set of 15 intermediate-band filters designed to do spectrophotometry. The available field of view is $58' \times 58'$, with a pixel scale of $1''.7$. The multicolor BATC filter system covers the total optical wavelength range from 3000 to 10 000 Å (see Fan et al. 1996; Zhou et al. 2001). The filters are specifically designed to avoid contamination from the brightest and most variable night sky emission lines. A full description of the NAOC Schmidt telescope,

Table 1. Parameters of BATC and U filter and statistics of observations.

No.	Name	cw[1] (Å)	Exp. (hr)	N.img[2]	rms[3]
1	BATC03	4210	00:55	04	0.024
2	BATC04	4546	01:05	04	0.023
3	BATC05	4872	03:55	19	0.017
4	BATC06	5250	03:19	15	0.006
5	BATC07	5785	04:38	17	0.011
6	BATC08	6075	01:26	08	0.016
7	BATC09	6710	01:09	08	0.006
8	BATC10	7010	01:41	08	0.005
9	BATC11	7530	02:07	10	0.017
10	BATC12	8000	03:00	11	0.003
11	BATC13	8510	03:15	11	0.005
12	BATC14	9170	05:45	25	0.011
13	BATC15	9720	06:00	26	0.009
14	U [4]	3665	00:50	02	–

[1] Central wavelength for each BATC filter.
[2] Image numbers for each BATC filter.
[3] Zero point error, in magnitude, for each filter as obtained from the standard stars.
[4] Images of U-band were obtained using thin CCD; Images of other bands were obtained using thick CCD.

CCD camera, data-acquisition system and definition of the BATC filter system can be found elsewhere (Fan et al. 1996; Zhou et al. 2003). To study the history of galaxy formation, images of M 33 covering its whole optical body were accumulated in a broad U-band and 13 intermediate-band filters, with a total exposure time of about 39.08 hours from September 23, 1995 to August 28, 2000. The CCD images are centered at RA $= 01^{\mathrm{h}}33^{\mathrm{m}}50^{\mathrm{s}}.58$ and Dec $= 30°39'08''.4$ (J2000). The dome flat-field images were taken by using a diffuse plate in front of the correcting plate of the Schmidt Telescope. For flux calibration, the Oke-Gunn primary flux standard stars HD 19445, HD 84937, BD+262606, and BD+174708 were observed during photometric nights. Because we had no calibration image for the U filter, we instead performed a model calibration developed specially for the BATC photometric system by Zhou et al. (1999). The parameters of the filters and the statistics of the observations are given in Table 1.

2.2. Image data reduction

The standard procedures of data reduction including bias subtraction, dark subtraction, flat-fielding, sky background fitting and flux calibration were performed. The flat-fielded images of each color were combined by integer pixel shifting. The cosmic rays and bad pixels were corrected by comparison of multiple images during combination. The images were recentered and position-calibrated using the *Hubble Space Telescope* (*HST*) Guide Star Catalog. The sky background subtraction will be specifically discussed in the next subsection. The absolute flux of intermediate-band filter images was calibrated using observations of standard stars. Fluxes, as observed through

Table 2. Two-dimensional SEDs in different filters for some areas of M 33 (10^{-30} ergs s^{-1} cm^{-2} Hz^{-1}).

X	Y	03	04	05	06	07	08	09	10	11	12	13	14	15	U
(1)	(2)	(3)	(4)	(5)	(6)	(7)	(8)	(9)	(10)	(11)	(12)	(13)	(14)	(15)	(16)
1121.	1034.	228.7	278.6	336.0	401.5	429.8	450.7	522.7	520.8	558.6	612.1	624.5	660.0	700.8	183.9
		5.4	4.3	4.2	4.5	3.9	4.9	4.2	6.2	8.0	8.0	10.5	14.0	16.3	15.0
1121.	1035.	231.0	279.5	338.6	404.5	432.7	454.7	528.8	524.5	562.0	615.1	625.4	662.6	710.7	184.0
		5.5	4.3	4.2	4.5	3.9	4.9	4.2	6.2	8.0	8.0	10.5	14.0	16.4	15.1
1121.	1036.	232.3	280.1	339.9	407.4	435.3	458.3	535.3	528.7	566.2	618.8	632.2	671.9	715.6	185.9
		5.5	4.3	4.2	4.5	3.9	5.0	4.2	6.3	8.0	8.0	10.6	14.1	16.5	15.1
1121.	1037.	234.3	280.3	340.3	411.3	437.3	462.0	541.3	534.4	569.9	619.3	638.3	676.1	718.1	186.9
		5.5	4.3	4.2	4.5	3.9	5.0	4.3	6.3	8.1	8.0	10.6	14.1	16.5	15.1
......															

BATC filters for the Oke-Gunn stars, were derived by convolving the SEDs of these stars with the measured BATC filter transmission functions (Zhou et al. 2001). Column (6) in Table 1 gives the zero-point error, in magnitudes, for the standard stars in each filter. The formal errors we obtain for these stars in 13 BATC filters are $\lesssim$0.02 mag. This indicates that we can define the standard BATC system to an accuracy of $\lesssim$0.02 mag.

2.3. Sky background subtraction

Since M 33 nearly fills the image frame, the sky background cannot be performed by the method used before (Zheng et al. 1999; Wu et al. 2002). We adopt a plane fitting method in this paper. In an image frame, three parts, the top left, top right and bottom left, were selected to perform the sky background fitting, because they are less contaminated by the light of M 33. Using these three parts, we experimented with MIDAS software to fit the sky background with a slope plane. All the image frames except the ones of the BATC11 and 12 bands were successfully background subtracted. For the image frames in BATC 11 and 12, because of their low quality of flat-fielding, the background-subtracted images were still not satisfactory. Thus, after the procedure above, small modifications of flat-fielding were applied on these two frames. We eliminated the central region (radius = 28′), where the main object of M 33 lies, from the images of BATC11 and BATC12 subtracted by BATC10, and then performed the sky background fitting with a two-dimensional Legendre polynomial of two orders. The two resulting two-dimensional curve surfaces were used to correct the sky background of BATC11 and BATC12, respectively.

2.4. Smoothing of images

Because the signal-to-noise ratio (S/N) decreases from the center to the edge of the galaxy, we smoothed the images with a boxcar filter. We masked the stars and background galaxies with PIPELINE II before smoothing (shown as the black circles in Fig. 4). The window sizes of the boxcar were selected depending on the ADU values of the BATC10 band image (7010 Å). If the ADU value was less than 100, the pixel was set to zero; if the value was higher than 100, the pixel was

adaptively smoothed by a boxcar filter of $N \times N$ (cell size), where

$$N = 75/(\mathrm{ADU}_{\mathrm{BATC10}})^{\frac{1}{2}}. \qquad (1)$$

By this method, the images were smoothed depending on the S/N of each cell. In the high flux area, the original pixels were used, whereas near the edge of M 33 the mean value of multiple pixels (cells) were used; as a result, the spatial resolution decreased from the center to the outer edge.

Finally, two-dimensional SEDs of M 33 can be obtained. The ADU value of each image was converted into units of 10^{-30} ergs s^{-1} cm^{-2} Hz^{-1}. As a example, we present some SEDs for different areas of M 33 listed in Table 2. Columns (1) and (2) show the (X, Y) positions of the photometric center of the regions, in units of pixel. Columns (3)–(16) present the fluxes in 14 filters, in units of 10^{-30} ergs s^{-1} cm^{-2} Hz^{-1}. The second line of each area is the uncertainty of flux in the corresponding band.

3. Data of evolutionary synthesis model

PEGASE is an evolutionary spectral synthesis model for starbursts and evolved galaxies of the Hubble sequence. It is continuous over an exceptionally large wavelength range from 220 Å up to 50 000 Å. It was extended to the near-infrared (NIR) of the atlas of synthetic spectra of Rocca-Volmerange & Guiderdoni (1988) with a revised stellar library including cold star parameters and stellar tracks extended to the thermally-pulsing regime of the asymptotic giant branch (TP-AGB) and the post-AGB (PAGB) phase. The synthetic stellar spectral library is taken from Kurucz (1992), modified by Lejeune et al. (1997) to fit the observed colors. A set of reference synthetic spectra at $z = 0$, to which the cosmological k- and evolution e- corrections for high-redshift galaxies are applied, is built from fits of observational templates (Fioc & Rocca-Volmerange 1997).

3.1. Theoretical spectral energy distributions of PEGASE

With the PEGASE code, we can compute the stellar SEDs of starbursts and evolved galaxies of the Hubble sequence at

Table 3. Scenarios of constant star formation.

IMF: Salpeter (1955)
Evolutionary tracks: "Padova"
Fraction of close binary systems: 0.50000E−01
Initial metallicity: 0.00000E+00
No infall
Constant star formation
Consistent evolution of the stellar metallicity
Mass fraction of substellar objects: 0.00000E+00
No galactic winds
Nebular emission
Extinction for a disk geometry:
Specific Inclination: 0.56000E+02

any stage of evolution, within the metallicity range $Z = 10^{-4}$ to 10^{-1}. Some factors, such as nebular emissions and dust effects, are considered. Typical parameters of PEGASE are the SFR and IMF.

Some SFRs, instantaneous burst, a constant and a series of Exp ($\tau = 1−15$ Gyr) star formation scenarios are taken into account in our work. Only the constant and Exp ($\tau = 12$ Gyr) star formation scenarios are satisfactory. Even for the many HII regions in M 33, where there are many emission lines, it can be well fit but this is not so for the other SFRs. The IMF is assumed to follow the Salpeter (1955) form, $\Phi(M) = A \times M^{-\alpha}$ with $\alpha = 2.35$ and a lower cutoff of $M_l = 0.1\ M_\odot$ and an upper cutoff $M_u = 125\ M_\odot$ (Sawicki & Yee 1998).

Assuming a standard IMF, SFR and other initial conditions, such as nebular emission and extinction, the PEGASE code can give an evolutionary history and some other important properties of a galaxy. The initial parameters of the constant star formation used in our work are given in Table 3.

3.2. Flux ratios of PEGASE

To determine the age distribution of M 33 and its evolutionary history, we attempt to find the best match between observed colors and predictions of PEGASE for each cell of M 33. Since the observational data have integrated luminosity, to make comparisons, we first convolve the SEDs of PEGASE with a BATC filter transmission curve to obtain the integrated luminosity. The integrated luminosity of the ith BATC filter $L_{\lambda_i}(t)$ can be calculated with

$$L_{\lambda_i}(t) = \frac{\int F_\lambda(t)\varphi_i(\lambda)\mathrm{d}\lambda}{\int \varphi_i(\lambda)\mathrm{d}\lambda}, \tag{2}$$

where $F_\lambda(t)$ is the flux of PEGASE at age t, and $\varphi_i(\lambda)$ is the transmission curve of the ith filter of BATC filter system.

For convenience, as we do in our series of work on galactic structure (Kong et al. 2000; Ma et al. 2001, 2002a,b), we use flux ratios that are independent of distance. We calculate the flux ratio of PEGASE, the integrated luminosity of BATC i

relative to that of BATC08 ($\lambda_8 = 6075$ Å) (thereafter the flux ratio),

$$C_{\lambda_i}(t) = L_{\lambda_i}(t)/L_{6075}(t). \tag{3}$$

4. Fitting algorithm and results

To study the integrated properties of the stellar populations in M 81 and clusters in M 33, Kong (2000) and Ma (2001, 2002a,b) used the simple stellar populations (SSPs) of the Galaxy Isochrone Synthesis Spectra Evolution Library (Bruzual & Charlot 1996). An SSP is defined as a single generation of coeval stars with fixed parameters, such as metallicity, IMF, etc. (Buzzoni 1999). As the basic building blocks of synthesis spectra of galaxies, SSPs can be used to infer the formation and subsequent evolution of the parent galaxies (Jablonka et al. 1996). Although SSPs are simple and reasonably well understood, they are still relatively rough for describing evolved galaxies. As a whole, a galaxy is not just a simple composition of SSPs, but one that has been formed with multiple generations of stellar populations. PEGASE can give the evolved SEDs of stellar populations by convolving SSPs with the adopted star formation history. In this section, some parameters for M 33 are determined by a χ^2-minimization method.

4.1. Reddening correction

Extinction affects intrinsic colors of M 33 and hence accurate ages, so the photometric measurements must be dereddened before the fitting procedure. The observed colors are affected by two main sources of reddening: (1) the foreground extinction in our Milky Way and (2) internal reddening due to varying optical paths through the disk of the parent galaxy (the intergalactic extinction is not considered here). We correct the foreground extinction to the observed colors of M 33 and consider internal extinctions in the PEGASE model so that we can compare the two colors with a consistent reddening condition. For the foreground extinction, McClure & Racine (1969) have measured the foreground color excess, $E(B - V) = 0.03 \pm 0.02$ for M 33, which we adopt here. In addition, we adopt the extinction curve presented by de Vaucouleurs et al. (1976). An extinction correction $A_\lambda = R_\lambda E(B - V)$ is applied, here R_λ is obtained by interpolating using the data of de Vaucouleurs et al. (1976). For the internal reddening of the galaxy, we take into account the disk extinction in the PEGASE model, then get the model SEDs after extinction. The geometry for the disk extinction is modelled by a uniform plane-parallel slab (Guiderdoni & Rocca-Volmerange 1987).

4.2. Model fits

By minimizing the differences between a set of intrinsic and synthetic SEDs, the best-fit evolutionary history of M 33 can be found. The method is computed using:

$$\chi^2 = \frac{1}{d}\sum_{i=3}^{16}\left[\frac{C_{\mathrm{int}}(\lambda_i) - C_{\mathrm{mod}}(\lambda_i, t)}{\sigma(\lambda_i)}\right]^2. \tag{4}$$

$C_{mod}(\lambda_i, t)$ is the flux ratio in the ith filter of a PEGASE model at age t. $C_{int}(\lambda_i)$ represents the intrinsic flux ratio for a cell of M 33. $\sigma(\lambda_i)$ is the ith uncertainty in the observed flux ratio. d is the number of degrees of freedom.

In this paper, an instantaneous burst, a constant and a series of Exp SFRs are tested. For Exp SFRs, SFR$(t) \propto \exp(-t/\tau)$, we have explored the values $\tau = 1-15$ Gyr. The match between observed colors of M 33 and predictions of the model is best when the timescale of star formation $\tau = 12$ Gyr. Among the three types of SFRs, the constant and Exp ($\tau = 12$ Gyr) SFR are found to best describe the evolutionary history of M 33. It is also found that in our fitting process, for most of M 33, the two models give very similar fitting results, except that the ages for the constant are larger than that for the Exp model. This estimate is consistent with previous studies. For example, Diaz & Tosi (1984) found an almost constant SFR in their numerical chemical evolution model; for Sc- and Sd-type spiral galaxies, $\tau = 15$ and 30 Gyr are used in Hyperz code (Bolzonella et al. 2000); Möller (1997) studied metallicity indicators by modelling Sc- and Sd-type spiral galaxies with $\tau = 9$ and 10.5 Gyr; Cornett et al. (1994) also obtained reasonable fits with constant and Exp star formation, the latter approach yielding $\tau = 3-5$ Gyr for a fixed age of 10 Gyr. We differ from the Cornett et al. approach to fitting Exp SFRs in which we solve for the age when the stellar populations first formed by fixing τ, whereas Cornett et al. fix the age and leave τ variable.

Figure 2 shows some plots of the best fits of flux ratios of PEGASE models with that for each cell of M 33. In Fig. 2, solid lines represent flux ratios of PEGASE models for the constant, dashed lines for the instantaneous burst and dotted lines for the Exp SFR; filled circles represent the intrinsic flux ratio of a cell of M 33. From this figure, we can see that the flux through the BATC09 filter includes line emission, primarily from Hα, which is most sensitive to recent star formation. The instantaneous burst models are least able to account for this emission while fitting the remaining SEDs. It is clear that, at most evolutionary stages of M 33, both the constant and Exp model present good matches between observed and theoretical SEDs. This also can be seen in Fig. 2.

4.3. Age distribution and evolutionary history

Figure 3 presents the age histograms of M 33 for the constant and Exp star formation models. The solid histogram represents the age distribution for the constant and the dotted one for the Exp model. Taking the constant model as an example, we analyze the age distribution and the evolutionary history, since the fitting results and age distribution of the two models are similar. The results show that, in general, M 33 has been forming stars continuously for the last $1-13$ Gyr, with most stellar populations less than 9 Gyr old. The stellar populations with ages from 7 to 8 Gyr are the main components of the galaxy.

For convenience, we define the "*central (region1)*" area as the region in the smallest rectangle, "*region2*" between the smallest and the second largest one, and "*region3*" between second largest and the largest one. Figure 4 shows the map of the age distribution of M 33. It is obtained by replacing the

Table 4. Comparison of age distributions of M 33 for two models.

Region	Age (Gyr)	
	Constant	Exp ($\tau = 12$ Gyr)
Region 1	$\gtrsim 10$	$\gtrsim 8$
Region 2	8	6
Region 3	7	5
Spiral arms	$\lesssim 5$	$\lesssim 3$

ADU of each pixel (cell) in the map with its corresponding fitted age. Light gray represents the old zones and dark gray the young ones. It clearly indicates that the stellar populations in the central regions are older than those in the outer regions, and that the youngest components reside in the spiral arms. There is an age gradient from the center to the edge of the galaxy. The age in the innermost central region is greater than $\gtrsim 10$ Gyr. In the area of *region2*, the mean age is about 8 Gyr. The stellar components in *region3* are younger than those in *region2*. The mean age for the stellar components in *region3* is about 7 Gyr, and for stars at the edge of *region3* is about 6 Gyr. We can see that the ages for the stellar populations in the spiral arms are even younger than the inner areas, $\lesssim 5$ Gyr. Some well-known giant HII regions, such as NGC 604, NGC 595, NGC 592 etc., can be clearly seen in the map. They are all very young, and their mean ages are less than 500 Myr. Comparing Fig. 4 to the (UV–Optical) images and radial color profiles shown in Marcum et al. (2001), we find that the radial gradient in age is consistent with the (UV–Optical) color gradients of Marcum et al. The age distribution for the Exp SFR is similar to that for constant star formation except for the younger ages for most areas of M 33. The comparison of age distributions of M 33 for the two models is shown in Table 4.

5. Comparison with the *UBVRI* filter system

To determine the dependence of the uncertainty of fitted ages on photometric errors, using a Monte Carlo simulation, we built a catalog containing simulated spectra of galaxies at different evolutionary stages from 1 to 10 Gyr for the constant SFR. Suppose that typical photometric errors in different filters are 0.02, 0.05 and 0.08 mag, and they are distributed as a Gaussian (normal) distribution. To compare BATC to the *UBVRI* filter systems, a sample of 2250 known-age simulated SEDs is obtained from the catalog by using a total of 20 filters (15 BATC and 5 *UBVRI* filters) simultaneously. It is thus guaranteed that the comparison of SEDs for the two systems is done for the same sample with the same age. The fitted ages of 2500 SEDs, for the BATC and *UBVRI* system respectively, are then obtained with the least-square procedure. Figure 5 shows the relations between the catalog ages and fitted ages (age$_{cat}$ vs. age$_{fit}$) with uncertainties of 0.02, 0.05 and 0.08 mag.

The standard deviation of the estimation σ_{age} is given by

$$\sigma_{age}^2 = \sum_{i=1}^{N} \frac{(age - \langle age \rangle)^2}{N-1}, \qquad (5)$$
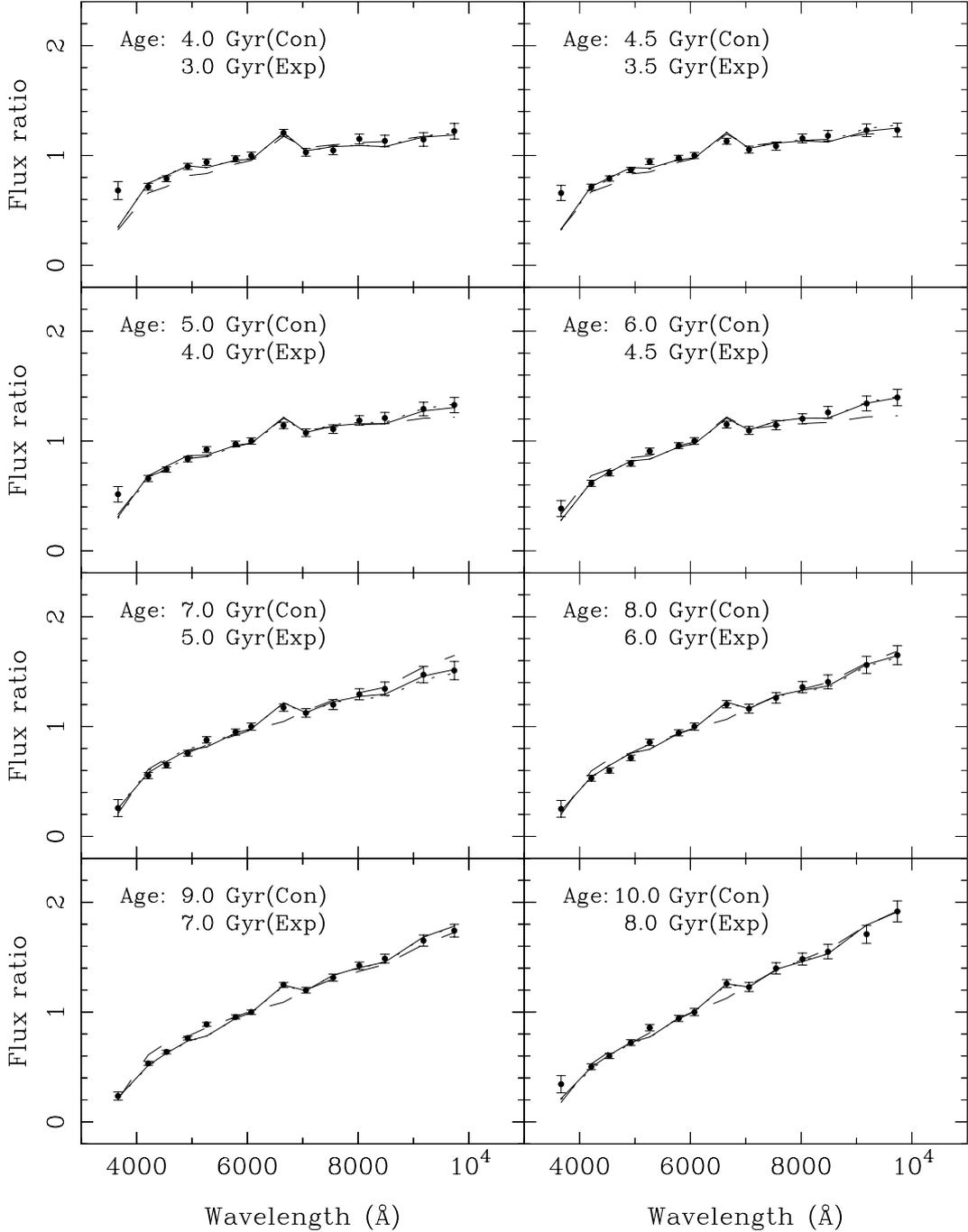
where N is the number of simulated spectra.

Fig. 2. The best fits of flux ratios of PEGASE models with that for a cell of M 33. Solid lines represent flux ratios of PEGASE models for the constant, dashed lines for the instantaneous burst and dotted lines for the Exp ($\tau = 12$ Gyr) SFR; filled circles represent intrinsic flux ratios for a cell of M 33.

From Fig. 5, we can see the advantage of the BATC over *UBVRI* system. For $\Delta m = 0.02$ mag, the performance is $\sigma_{age} = 0.047$ Gyr for BATC system and $\sigma_{age} = 0.095$ Gyr for *UBVRI* system; for $\Delta m = 0.05$ mag, the performance is $\sigma_{age} = 0.140$ Gyr for BATC system and $\sigma_{age} = 0.226$ Gyr for *UBVRI* system; for $\Delta m = 0.08$ mag, the performance is $\sigma_{age} = 0.209$ Gyr for BATC system and $\sigma_{age} = 0.357$ Gyr for *UBVRI* system. At the same level of uncertainty, the deviation for the BATC system is smaller than *UBVRI* system. The performance of the BATC system with even larger

observational uncertainty $\Delta m = 0.08$ mag is still better than *UBVRI* system with the uncertainty $\Delta m = 0.05$ mag. Figure 5 also shows a large dispersion of observational uncertainties for the *UBVRI* system. This is due to the smaller number and larger bandwidth of the filters, which make it less sensitive to delicate spectral features. For the BATC system, the 15 filters and their intermediate bandwidth create a distinct advantage. More detailed spectral features can be sensed. For example, some important emissions, such as [OIII]$_{\lambda 5007}$, Hα, Hβ, [NII]$_{\lambda 6583}$, [SIII]$_{\lambda 9069}$, can be easily observed by the
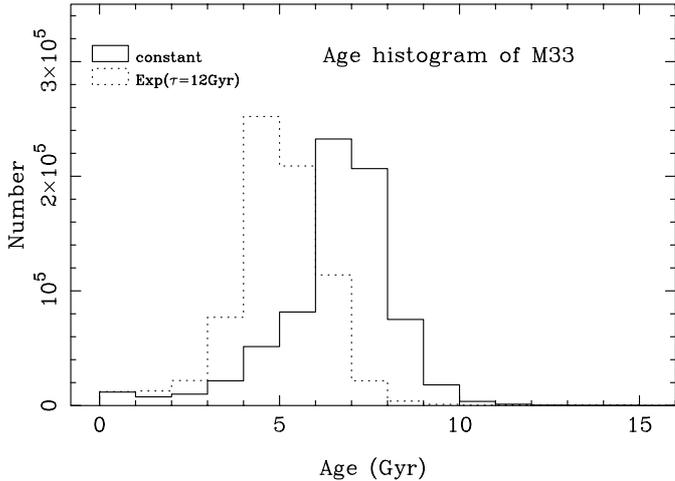
Fig. 3. Age histogram of M 33 for the constant and Exp star formation. Solid line represents the age distribution for the constant and dotted one for the Exp star formation.

filters of BATC05 ($\lambda = 4925$ Å), BATC09 ($\lambda = 6710$ Å) and BATC13 ($\lambda = 9182$ Å) etc. So the intermediate-band spectrophotometry of BATC improves much on the broad-band photometry of *UBVRI* in presenting delicate SEDs of a galaxy, especially for a galaxy such as M 33, which is rich in line emission.

6. Summary and conclusions

In this paper, we have obtained the SEDs of M 33 in 14 colors with the NAOC 60/90 cm Schmidt telescope. Our main conclusions are:

1. Multicolor images of the spiral galaxy M 33 are obtained in the BATC photometric system. The SEDs for each area in M 33 are derived after the standard procedure of data reduction for the BATC program, which include bias substraction, dark subtraction, flat-fielding, sky background fitting and flux calibration.

2. With help of the evolutionary synthesis code PEGASE we build galaxy evolutionary models, such as the instantaneous burst, constant and a series of Exp ($\tau = 1{-}15$ Gyr) star formation models that include some parameters and initial conditions. By fitting the flux ratio of each cell of M 33 with these models, we find that M 33 could be best described with the constant and Exp ($\tau = 12$ Gyr) star formation models.

3. For the constant model, from the two-dimensional age distribution of M 33, we find that the mean ages of the stellar populations in the central regions are older than those in the outer regions, which suggests that the star formation in the central regions occurred earlier than the outer regions; formation of the stellar populations in the spiral arms is the most recent, which shows that a large number of stars are forming now. It also can be shown that star formation in M 33 has occurred almost continuously from $1{-}13$ Gyr, and most of the observed stellar populations in it are less than 9 Gyr. The stars, with ages from 7 to 8 Gyr, are the
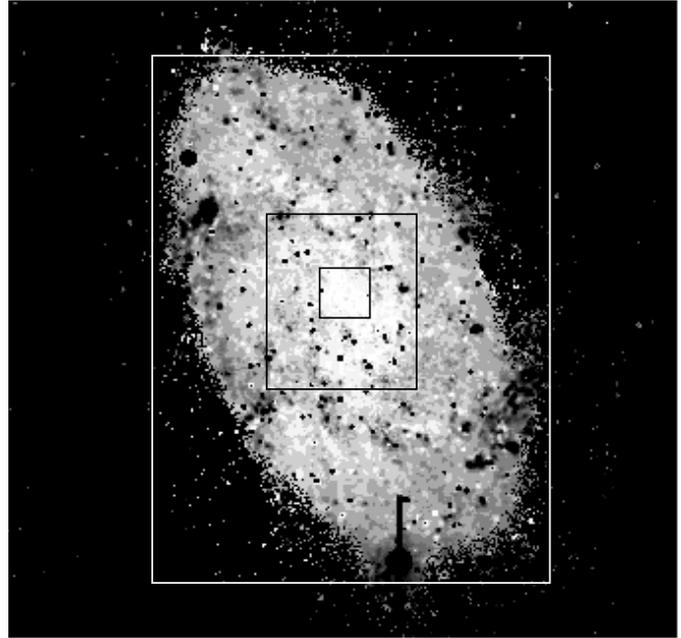

Fig. 4. Map of the age distribution of M 33 for constant star formation. Light gray corresponds to the old and dark gray to the young zones. The black spots represent the masked regions, such as most of the foreground stars, some HII regions and background galaxies.
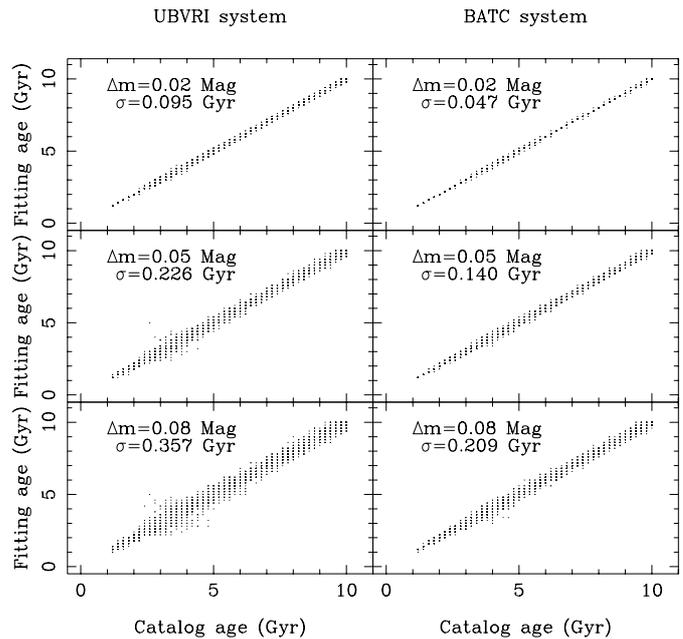

Fig. 5. Map of the relation of the catalog ages and fitted age (age$_{\mathrm{cat}}$ vs. age$_{\mathrm{fit}}$) for the *UBVRI* system (*left*) and BATC system (*right*) with photometric errors of 0.02, 0.05 and 0.08 mag, respectively. The range of catalog ages is from 1 to 10 Gyr.

main components of the galaxy. A similar age distribution can be obtained with the Exp model except for smaller initial ages for most areas of M 33.

References

Bolzonella, M., Miralles, J. M., & Pelló, R. 2000, A&A, 363, 476

Bressan, A., Chiosi, C., & Tantalo, R. 1996, A&A, 311, 425

Bruzual, G., & Charlot, S. 1993, ApJ, 405, 538

Bruzual, G., & Charlot, S. 1996, Documentation for GISSEL96 Spectral Synthesis Code

Bruzual, G., & Charlot, S. 2003, MNRAS, 344, 1000

Buzzoni, A. 1999, in Cosmological Parameters and the Evolution of the Universe, ed. K. Sato, IAU Symp., 183, 18

Chandar, R., Bianchi, L., & Ford, H. C. 1999, ApJS, 122, 431

Charlot, S., & Bruzual, G. 1991, ApJ, 367, 126

Chiosi, C., Bressan, A., Portinari, L., & Tantalo, R. 1998, A&A, 339, 355

Cornett, R. H., O'Connell, R. W., Greason, M. R., et al. 1994, ApJ, 426, 553

de Vaucouleurs, G., de Vaucouleurs, A., & Corwin, H. 1976, Second Reference Catalogue of Bright Galaxies (Austin: Univ. Texas Press)

Diaz, A. I., & Tosi, M. 1984, MNRAS, 208, 365

Fan, X. H., Burstein, D., Chen, J. S., et al. 1996, AJ, 112, 628

Fioc, M., & Rocca-Volmerange, B. 1997, A&A, 326, 950

Fioc, M., & Rocca-Volmerange, B. 2000
    [arXiv:astro-ph/9912179]

Freedman, W. L., Wilson, C. D., & Madore, B. F. 1991, ApJ, 372, 455

Guiderdoni, B., & Rocca-Volmerange, B. 1987, A&A, 186, 1

Hodge, P. W., Balsley, J., Wyder, T. K., & Skelton, B. P. 1999, PASP, 111, 685

Jablonka, P., Bica, E., Pelat, D., & Alloin, D. 1996, A&A, 307, 385

Kennicutt, R. C. 1998, ARA&A, 36, 189

Kewley, L. J., Dopita, M. A., Sutherland, R. S., Heisler, C. A., & Trevena, J. 2001, ApJ, 556, 121

Kong, X., Zhou, X., Cheng, J. S., et al. 2000, AJ, 119, 2745

Kurucz, R. L. 1992, Model Atmospheres for Population Synthesis, ed. B. Barbuy, & A. Renzini, The stellar population of Galaxies (Dordrecht: Reidel), IAU Symp., 149, 225

Leitherer, C., Schaerer, D., & Goldader, J. D., et al. 1999, ApJS, 123, 3

Lejeune, Th., Cuisinier, F., & Buser, R. 1997, A&AS, 125, 229

McClure, R. D., & Racine, R. 1969, AJ, 74, 1000

Ma, J., Zhou, X., Kong, X., et al. 2001, AJ, 122, 1796

Ma, J., Zhou, X., Chen, J. S., et al. 2002a, AJ, 123, 3141

Ma, J., Zhou, X., Chen, J. S., et al. 2002b, A&A, 385, 404

Marcum, R. M., O'Connell, R. W., Fanelli, M. N., et al. 2001, ApJS, 132, 129

Möller, C. S., Fritze-v. Alvensleben, U., & Fricke, K. J. 1997, A&A, 317, 676

Rocca-Volmerange, B., & Guiderdoni, B. 1988, A&AS, 75, 93

Salpeter, E. E. 1955, ApJ, 121, 161

Sawicki, M., & Yee, H. K. C. 1998, AJ, 115, 1329

Schaerer, D., & de Koter, A. 1997, A&A, 322, 598

Schaerer, D., & Vacca, W. D. 1998, ApJ, 497, 618

Searle, L., Sargent, W. L. W., & Bagnuolo, W. G. 1973, ApJ, 179, 427

Tinsley, B. M. 1972, A&A, 20, 383

Wu, H., Burstein, D., Deng, Z. G., et al. 2002, AJ, 123, 1364

Zheng, Z. Y., Shang, Z. H., Su, H. J., et al. 1999, AJ, 117, 2757

Zhou, X., Chen, J. S., Xu, W., et al. 1999, PASP, 111, 909

Zhou, X., Chen, J. S., Zhu, J., et al. 2001, ChJAA, 1, 372

Zhou, X., Jiang, Z. J., Ma, J., et al. 2003, A&A, 397, 361